MATERIALE PLASTICE
https://revmaterialeplastice.ro
https://doi.org/10.37358/Mat.Plast.1964

Study on Mechanical Properties and Constitutive Models of Epoxy Resin under Low Strain Rate Tension and Compression

CHANGLIN ZHAO[1]*, HAO LIU[2]*
[1] Department of Civil Engineering, Faculty of Engineering, Universiti Putra Malaysia (UPM), Serdang, Selangor, 43400, Malaysia
[2] School of Aerospace Engineering, Tsinghua University, Beijing, 100084, China

Abstract: *Epoxy resin (EP) can be flexibly bonded to various materials and has a wide range of applications in aerospace manufacturing. One of the most common applications is as a matrix phase in the preparation of advanced fiber composites. Therefore, it determines the mechanical properties of composites, particularly in view of the effect of differences in strength. To this end, we prepared tensile and compressive specimens of EP according to the ASTM standard and carried out quasi-static loading tests at different strain rates (0.001 to 0.1 s^{-1}). The results show that EP has an obvious strain rate dependence, and the elastic modulus, yield strength, and plastic flow platform in tension and compression have obvious differences. Furthermore, by fitting the experimental stress-strain curves in tension, we used the power function to establish a theoretical model in terms of yield stress and elastic modulus. Subsequently, the nonlinear constitutive models in the compressive state were established based on the Sherwood-Frost model. Thus, a complete constitutive model was obtained which takes into account both tensile and compressive differences. Based on these constitutive models, the tensile and compressive mechanical behaviors obtained by parameter inversion are in good agreement with their experimental results, proving that the developed constitutive models have good theoretical prediction capability. These research results provide a reference for the practical engineering application of EP, especially for the fiber-reinforced EP composites.*

Keywords: *Epoxy resin (EP), polymers, strength-differential material, mechanical behavior, constitutive model, strain rate effect*

1. Introduction

Epoxy resin (EP) is widely used in the aerospace industry as an electrical insulator to resist dust and moisture, and as a filler to provide electromagnetic shielding, due to its advantages such as easy processing, high safety, good toughness, corrosion resistance, and excellent adhesion [1–3]. In addition, with the development of additive manufacturing technology, the application of polymer plastics has been significantly promoted, and EP has also ushered in a new stage [4,5]. It is worth noting that one of the uses of EP is as a matrix for the production of advanced fiber composites like CFRP (carbon fiber reinforced plastic) and GFRP (glass fiber reinforced plastic). These composites boast excellent mechanical properties and are used in the design of lightweight, and high-strength functional structures, so it is significant to conduct research on the mechanical properties of EP.

With regard to the mechanical study of EP, Yao et al. [6] performed the tensile impact test of EP by SHPB (split Hopkinson pressure bar), where the results show that the strain rate has a significant influence on the tensile modulus, which is manifested by the stress-strain response gradually becoming nonlinear with increasing strain rate. Littell et al. [7] investigated the tensile, compressive, and torsional mechanical properties of Epon E862 at different strain rates. The results show that the mechanical response of EP is related to strain rate. In terms of Epon 828/T-403 and PMMA (polymethyl methacrylate), Chen et al. [8] investigated their quasi-static and dynamic behavior under uniaxial tensile

*email: gs69966@student.upm.edu.my; drhaoliu@tsinghua.edu.com

and compressive loading states. The experimental results show that the dynamic mechanical behavior of the two polymer materials under tension is different from the dynamic compression behavior. Besides, in the quasi-static experiment, the tensile and compressive strengths have an obvious difference, which is called the strength-difference effect. Cohen and Ishai [9] conducted some tests on EP composites to investigate the strain-rate dependence of the modulus of filled and porous epoxy composites. They found that the compressive modulus of both filled and porous EP systems increased with the increase in strain rate. Gómez-del Río et al. [10] added different types of nanoparticles, including SBM (poly methyl methacrylate), triblock copolymers (rubber nanoparticles), and carbon nanotubes (rigid nanofillers), to the EP system, analyzing its compressive properties at different strain rates. The results demonstrate that the mechanical properties of the modified EP are similar to those of pure EP. At a constant strain rate, the EP specimen showed an obvious yield stage followed by a stress drop [11]. Tamrakar et al. [12] investigated the strain rate-related mechanical properties of DER 353 EP under quasi-static (0.001 to 1 s^{-1}) and high-rate (1000 to 12,000 s^{-1}) compression loads and ambient temperature conditions. Their results reveal that the elastic modulus is related to strain rate, and the stress-strain response is softening after yielding, followed by plastic flow and strain hardening at lower strain rates. Zhong et al. [13] conducted tensile and compression tests on flame-retardant epoxy resin at different loading rates. The results showed that the mechanical properties of EP at low and medium loading rates were significantly affected by strain rate and the difference between tensile and compression.

Generally, the constitutive relationship is a mathematical expression used to describe the regularity of deformation of a material under external influences (such as stress, strain, etc.), which reflects the material mechanics. Through the constitutive relationship, we can predict the material behavior under different loading conditions, i.e., the material constitutive relationship is important. Zhu et al. [14] used SHPB to explore the viscoelastic behavior of EP at high strain rates (10^2 to 103 s^{-1}) and up to 7.5% strain, and proposed a simple and practical nonlinear thermo-viscoelastic constitutive equation, but the mechanical properties at low strain rates were not discussed. Ning [15] proposed an analytical expression of the stress-strain relationship and used this equation to fit the tensile results of twenty epoxy castings. The theoretical results were found to be in good agreement with the experimental results, but a complete constitutive model including tensile and compressive properties is lacking. Wu [16] studied the quasi-static compression behavior of TDE86 EP at four temperatures and three strain rates, and conducted a dynamic compression test using the SHPB. It was found that the dynamic stress-strain behavior of EP can be divided into four phases: the initial elastic section, yielding, strain softening, and unloading. Colak and Cakir [17] presented a constitutive equation for the rate- and temperature-dependent stress-strain behavior of amorphous polymers, which is an improvement on the cooperative viscoplastic theory based on the overstress model. Their model was shown to predict the quasi-static compression and high-strain-rate impact behavior of DER353 EP.

Furthermore, Theocaris [18] found that EP followed a linear viscoelastic law at a medium strain rate and within a certain time range in creep and relaxation tests at different temperatures without or with plasticizers. Zhao et al. [19] combined DSC (differential scanning calorimetry) curves and gel time-temperature curves to study the processing performance of the EP system in VARI, selecting 60°C as the cure temperature; and found that the temperature effect on mechanical properties under low-strain conditions is almost negligible. Sun et al. [20] established a micromechanical model of unidirectional composites; and used it to analyze the mechanism of compressive failure. They found that the compressive strength and failure mode of composites are mainly affected by the stress state of the matrix with a kink band. Zhao et al. [21] tested the tensile and compressive mechanical properties of hand-applied plain woven carbon fiber and EP. They found that the compression of EP must take into account the size effect of the sample, and that the size effect of the sample is not obvious under tension. Koerber et al. [22] studied the high-strain-rate characteristics of unidirectional carbon/EP IM7-8552 under transverse compression and in-plane shear loading. The results show that the Puck failure criterion can provide a good strength prediction under both quasi-static and dynamic loading. Xia et al. [23]

conducted mechanical tests on EP at different temperatures, and found that temperature enhanced the nonlinear behavior of the stress-strain relationship. They incorporated the temperature factor into the constitutive equation to realize the nonlinear behavior, but did not discuss the mechanical differences at various strain rates.

Recently, Liu et al. [24] pointed out that the tensile and compressive behavior of unidirectional GFRP laminates varies at medium and low strain rates. The result shows that the modulus and failure strength of unidirectional GFRP laminates are positively correlated with the loading rate. In an experimental research on carbon/EP composites related to strain rate effect, Gilat et al. [25] found that the deformation rate has an influence on the response of the IM7/977-2 EP system. This observation indicate that the sensitivity of composites to strain rate is driven by the EP behavior. However, there is a lack of research into the influence of different strain rates. At the same time, experimental data demonstrate that constitutive relations related to strain rate are necessary for the full prediction of polymer-based composites. Shokrieh and others [26] employed a high-speed servo-hydraulic tester to study the tensile failure modes of unidirectional glass/EP composites at strain rates from 0.001 to 100 s^{-1}. The results show that at low strain rates, the damage area covers a small part of the fracture surface, while as the strain rate increases, the damage path covers the whole standard section, and extensive debonding between the fiber and matrix is also observed. Zhang et al. designed a CFRP damping modification method based on the *in-situ* construction of a directional graphene oxide coating on the CF surface, and found that the intralayer slip between EP/fiber would preferentially convert into interlayer slip within the coating [27]. Moreover, many EP-based composites and structures have been studied, especially for the design of lightweight structures, such as the CFRP auxetic structures [28], the CFRP-aluminum foam composites [29], etc.

The above discussion shows that the current research on tensile and compressive properties of EP mainly discusses the two separately or does not establish constitutive equations or study high strain rates, but its complete constitutive model still needs further development [5–9,16–19]. To study the mechanical properties of EP under tensile and compressive loading and various strain rates, we have performed the low strain rate loading tests and developed constitutive models. Therefore, the main innovations of this paper are: preparing the standard specimens, revealing the mechanical behavior under different strain rates, and establishing the constitutive model with a strength-difference effect. Most importantly, the yield stress model in an exponential function form, the tensile constitutive model in a power function form, and the complete constitutive model have been established, providing a reference for studying the tensile and compressive behavior of EP and its composites.

2. Material preparation and test methods

2.1. Preparation of EP specimens

The EP casting system was prepared using E-51 liquid reagent. The preparation process was as follows: The EP and the curing agent were mixed at a mass ratio of 5:1, poured into the mould, and then heated to 140°C for 12 h. After cooling, demolding was performed to obtain the corresponding EP specimens. Figure 1a shows the tensile specimens and Figure 1b shows the compression specimens. The cross-section of the compression sample is square or circular. The gauge section size of the EP tensile sample is length × width × thickness of 60 mm × 4 mm × 10 mm, in accordance with the ASTM D638-22 standard. The length × diameter of the circular EP compression specimen is 25 mm × 10 mm, which complies with the ASTM D695-15 standard. The length × side length of the square EP compression specimen is 25 mm × 10 mm, which also complies with the ASTM D695-15 standard.

2.2. Quasi-static test methods

The experiments are performed using a CSS44300-MTS universal electronic testing machine, which can conduct tensile and compression tests. The experiments are in a quasi-static mode, with a low strain rate in the range of 0.001 to 0.1 s^{-1}. The experimental parameters are shown in Table 1, and the loading

and installation site is shown in Figure 2. For the tensile tests, the loading strain rates are 0.001, 0.01, and 0.1 s^{-1}, respectively. For the compression tests, the loading strain rates are 0.001, 0.01, 0.05, and 0.1 s^{-1}, respectively. The experimental data are collected using Test Expert Version 3.6. The mechanical behavior of EP is analyzed using the collected force-displacement curves and the observed damage conditions.

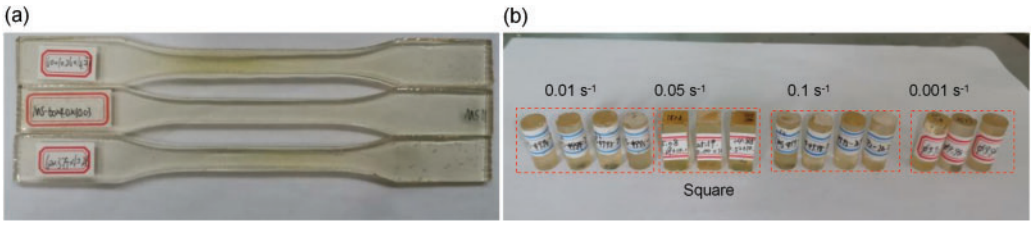

Figure 1. EP tensile specimens (a), and compression specimens (b) including circular and square cross sections

Table 1. Experimental information

Type	Loading rate (mm/min)	Repetitions	Strain rate (s^{-1})
Tensile test	3.6	3	0.001
	36	3	0.01
	360	3	0.1
Compression test	1.5	3	0.001
	15	4	0.01
	75	3	0.05
	150	4	0.1

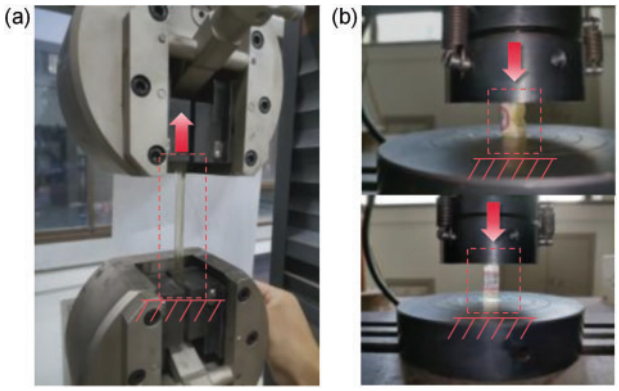

Figure 2. Specimen installation during (a) the tensile process, and (b) the compression process including circular and square specimens

Here, the true stress-strain relationship was used to express the mechanical properties of EP [30]. In the equations, the subscript T was adopted to represent true stress and strain, and the subscript e is used to represent engineering stress and strain. According to the definitions of stress and strain, the force-displacement curves are converted into engineering stress σ_e and strain ε_e, and then converted into true stress and strain. The strain rate $\dot{\varepsilon}$ is calculated as follows:

$$\dot{\varepsilon} = \frac{v}{l} \tag{1}$$

The calculation equation for engineering stress is

$$\sigma_e = \frac{F_i}{A_i} \tag{2}$$

The calculation equation of engineering strain is

$$\varepsilon_e = \frac{\Delta l_i}{L_i} \tag{3}$$

In the above equations, v represents the loading speed, l represents the original length of the specimen, F represents the tensile or compressive force, A represents the cross-sectional area of the specimen, L represents the original length of the specimen, Δl_i represents the change in length of the specimen after being subjected to F, and i represents the i-th independent repeated test.

The calculation equation of true stress σ_T and strain ε_T is

$$\begin{cases} \sigma_T = (1 + \varepsilon_e)\sigma_e \\ \varepsilon_T = \ln(1 + \varepsilon_e) \end{cases} \tag{4}$$

The calculation equation of elastic modulus E is

$$E = \frac{\sigma_T}{\varepsilon_T} \tag{5}$$

3. Experimental results and discussion

3.1. Tensile mechanical properties

The force-displacement curves of the EP tensile specimen are shown in Figure 3. In order to improve the reliability and accuracy of the experimental results, we repeated the independent experiment 3 to 4 times at each loading rate, and calculated the average value at each loading rate as the experimental result describing the mechanical properties of EP. At the strain rate of 0.001 s^{-1}, the force-displacement curves of the three EP specimens have good repeatability (Figure 3a). When the tensile load reaches about 2200 N, the specimen breaks; when the strain rate is 0.01 s^{-1}, the specimen breaks when the tensile load reaches about 880 N (Figure 3b); when the strain rate is 0.1 s^{-1}, the specimen breaks when the tensile load reaches about 800 N (Figure 3c). During the experiment with a strain rate of 0.1 s^{-1}, the specimen broke at the clamping end due to the clamping problem. Therefore, the experimental data of specimen ③ is not referenceable. Here, specimen ③ is discarded and only the average of test results ① and ② is calculated. The test results show that the maximum load-bearing capacity of EP during tension decreases with the increase of strain rate. During the tensile process, it can be seen that the mechanical behavior of EP before failure is mainly linear elastic, but a nonlinear segment is observed in the initial stage, which may be caused by slip and instability at the specimen's clamped end. At the same time, the load of EP suddenly dropped when the tensile load reached the material failure limit, which is similar to the results in [11].

The engineering stress-strain curves at different strain rates were calculated according to Eqs. (2) and (3), as shown in Figure 3d. The true stress-strain curve was obtained using Eq. (4) [30]. As can be seen from Figure 3d, the loading process can be divided into two stages, the initial nonlinear stage and the linear elastic stage, but the nonlinear segment is caused by the experimental process and will not be discussed here. When the load reaches the yield stress of EP, the specimen breaks and fails. According to Eq. (5), the elastic modulus of the material at different strain rates can be calculated, namely $E_{t0.001} = 763.236$ MPa, $E_{t0.01} = 840.333$ MPaand $E_{t0.1} = 848.000$ MPa, respectively. Here, the subscript "t" represents the tensile state. It can be seen that the modulus of EP gradually increases

with the increase of strain rate under tensile conditions. The yield stress of the material is $\sigma_{t0.001}$ = 49.624 MPa, $\sigma_{t0.01}$ = 20.014 MPa and $\sigma_{t0.1}$ = 17.633 MPa, respectively. It can be seen that the yield stress decreases with the increase of strain rate. Therefore, in the process of analyzing the tensile mechanical behavior of EP, it is necessary to consider the influence of the strain rate effect on the mechanical behavior.

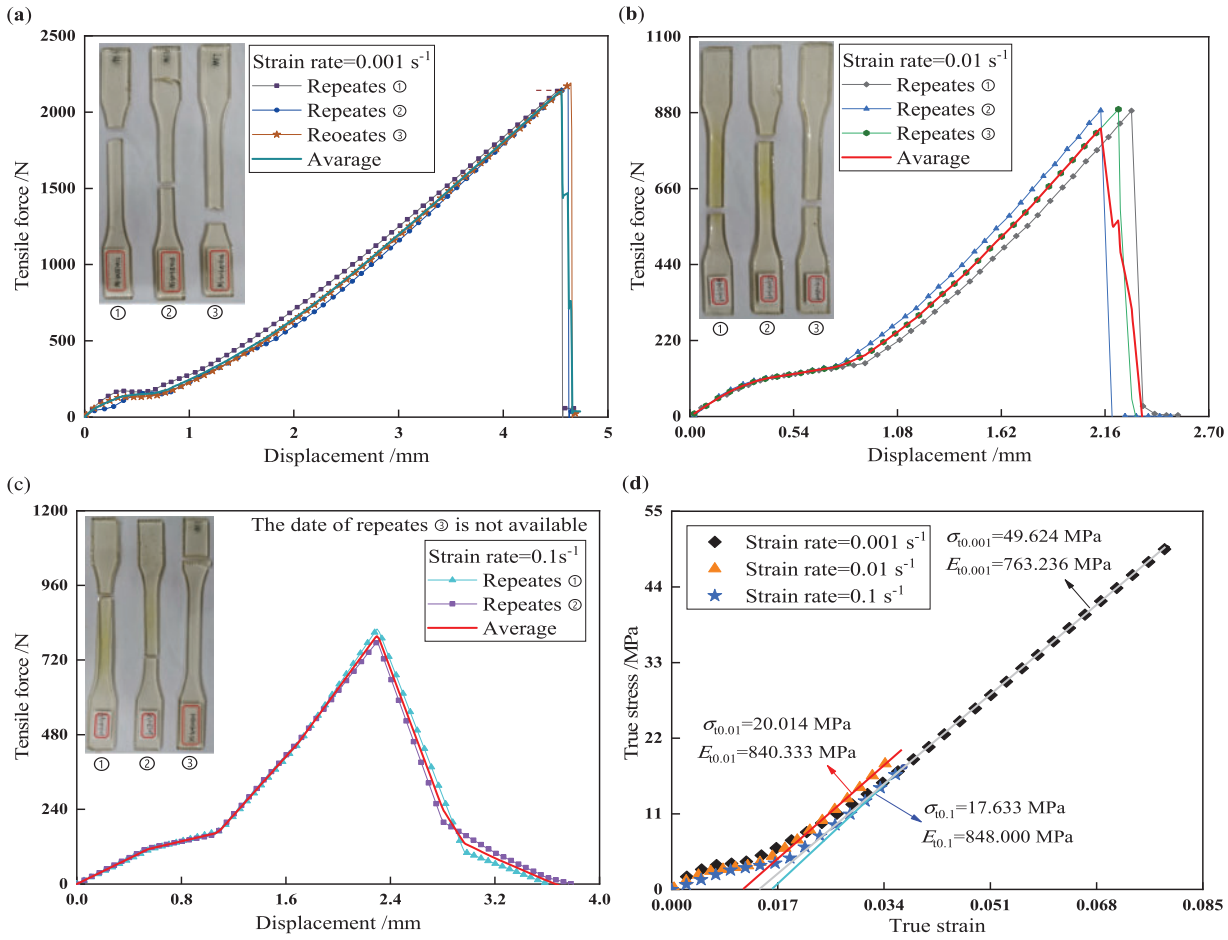

Figure 3. Tensile force-displacement curves of EP at strain rates of (a) 0.001 s^{-1}, (b) 0.01 s^{-1}, (c) 0.1 s^{-1}, and (d) stress-strain curves at these three strain rates including their extension lines

3.2. Compression mechanical properties

The force-displacement curves of EP under compression are shown in Figure 4. The stress-strain trends of the four strain rates are similar, including initial linear elasticity, yield, strain softening and unloading segments [17]. The mechanical behavior of the square-sectional specimens is similar to that of the circular-sectional specimens at strain rates of 0.01 and 0.1 s^{-1}, which shows that the influence of the cross-sectional shape is not significant, indicating that the experimental data of the square-sectional specimens can be used as a research object. Due to the process defects in the preparation of the specimen, there are some pores and pre-damage [31], the EP does not have perfect mechanical behavior. Therefore, under compression, a suitable representative is selected from independent experiments as the research object. When the strain rate is 0.001 s^{-1}, the repeatablity of ② and ③ is better, and the flow stress of ② is more, so this specimen is selected as the research object; when the strain rate is 0.01 s^{-1}, specimen ③ is selected as the object; when the strain rate is 0.1 s^{-1}, specimen ① is selected as the object; when the strain rate is 0.05 s^{-1}, specimen ① is selected as the object. The stress-strain curves at different strain rates were calculated and are shown in Figure 4e. EP exhibits linear elastic

behavior before reaching the yield point during compression, and the stress at the highest point is the failure limit under compression [32]. The stresses at different strain rates are $\sigma_{c0.001} = 114.082$ MPa, $\sigma_{c0.01} = 126.825$ MPa, $\sigma_{c0.05} = 127.780$ MPa and $\sigma_{c0.1} = 140.004$ MPa, respectively, where the subscript "*c*" indicates the compression state. The elastic modulus in compression are $E_{c0.001} = 1878.848$ MPa, $E_{c0.01} = 2240.105$ MPa, $E_{c0.05} = 2280.622$ MPa and $E_{c0.1} = 2801.874$ MPa, respectively. It can be found that under compression, as the strain rate increases, the yield strength and elastic modulus also increase, showing a positive correlation, which is consistent with the experimental results in [13]. Compared to the stress-strain curve under tensile loading, the stress-strain curve under compressive loading has the obvious feature of an additional nonlinear yield and strain softening stage [17].

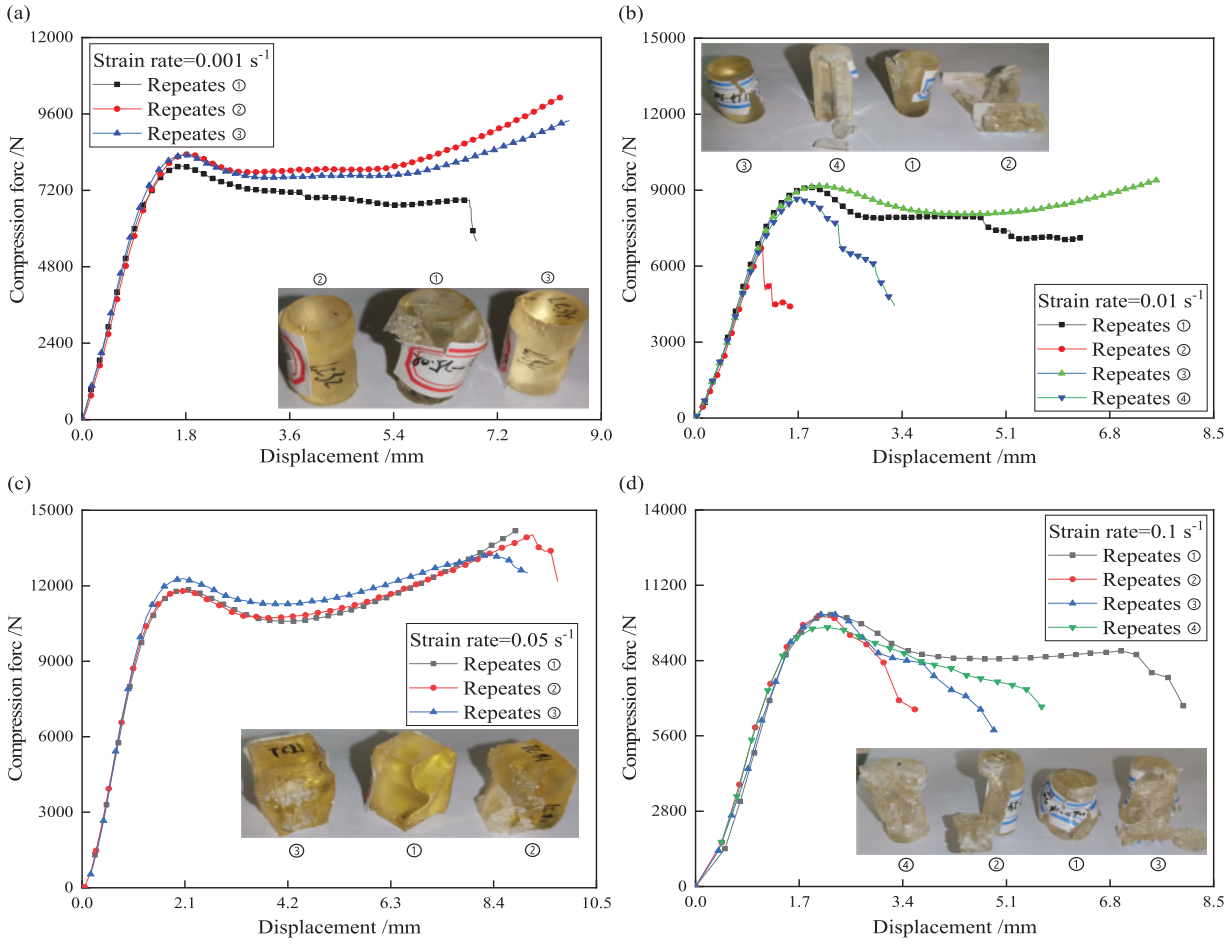

Figure 4. (Continued)

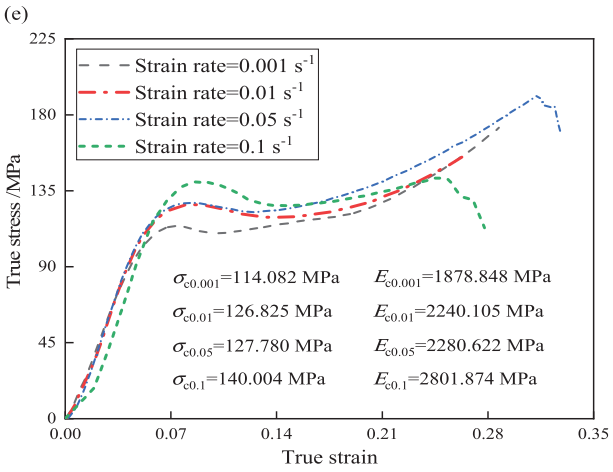

Figure 4. Force-displacement curves of EP under compression with strain rates of (a) 0.001 s^{-1}, (b) 0.01 s^{-1}, (c) 0.05 s^{-1}, (d) 0.1 s^{-1}, and (e) stress-strain curves at these strain rates

3.3. Failure analysis

From the tensile test results in Figure 3, it can be found that EP is a brittle material, but from the compression test results in Figure 4, it can be seen that EP also has a certain degree of viscoelasticity [14]. The failure morphology of the EP fracture surface under compression (0.001 s^{-1}) is shown in Figure 5. During the compressive loading process, obvious wrinkles appear on the outer contour of the specimens, and micro-cracks are gradually initiated in their vicinity. As the load increases, these micro-cracks rapidly expand to form more cracks, and finally fracture occurs. The brittle cross-section is relatively smooth, similar to previous studies [31].

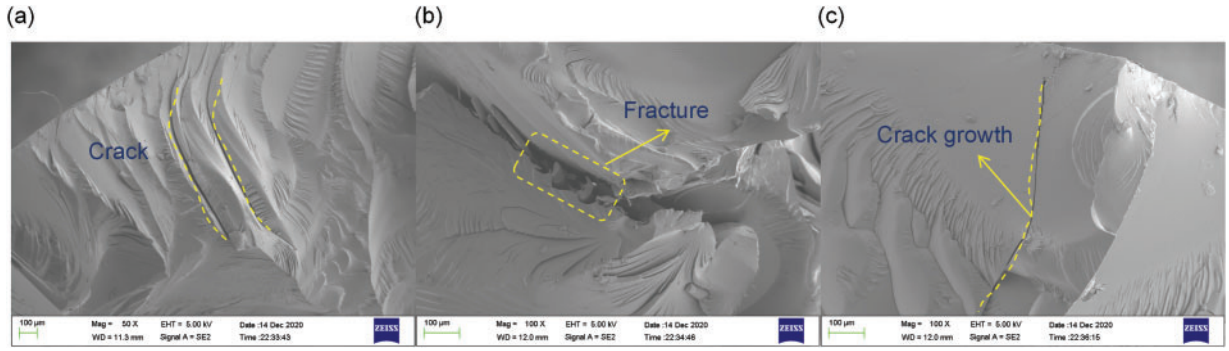

Figure 5. Microscopic morphology of the EP fracture surface taken from the compressed specimen at a loading rate of 0.001 s^{-1}

4. Establishment of constitutive model

4.1. EP yield stress model

Tensile and compressive loading are important due to their different mechanical behavior, and the influence of the strain rate effect must also be considered when establishing the constitutive model [24]. The strength of materials usually has a power law relationship [33], such as a logarithmic relationship. For this reason, the Allometric1 function was used to describe the yield stress of EP. The yield stress models under tension and compression are as follows:

$$\sigma_t = a_t \dot{\varepsilon}^{b_t} \tag{6}$$

$$\sigma_c = a_c \dot{\varepsilon}^{b_c} \tag{7}$$

where σ_t is the tensile yield stress of EP, σ_c is the compressive yield stress of EP, $\dot{\varepsilon}$ is the strain rate of EP in tension and compression, a and b are material constants determined by experiments, and the subscript '*t*' represents tension and '*c*' represents compression. Furthermore, the relationship between the yield stress and strain rate of EP in tension and compression can be obtained by fitting the experimental results as shown in Figure 6, and the material parameters are shown in Table 2. It is worth noting that the variance R_t^2 obtained by fitting is 0.923 and R_c^2 is 0.999, indicating that within a certain strain rate range, Eqs. (6) and (7) can be applied to describe the yield limit of EP.

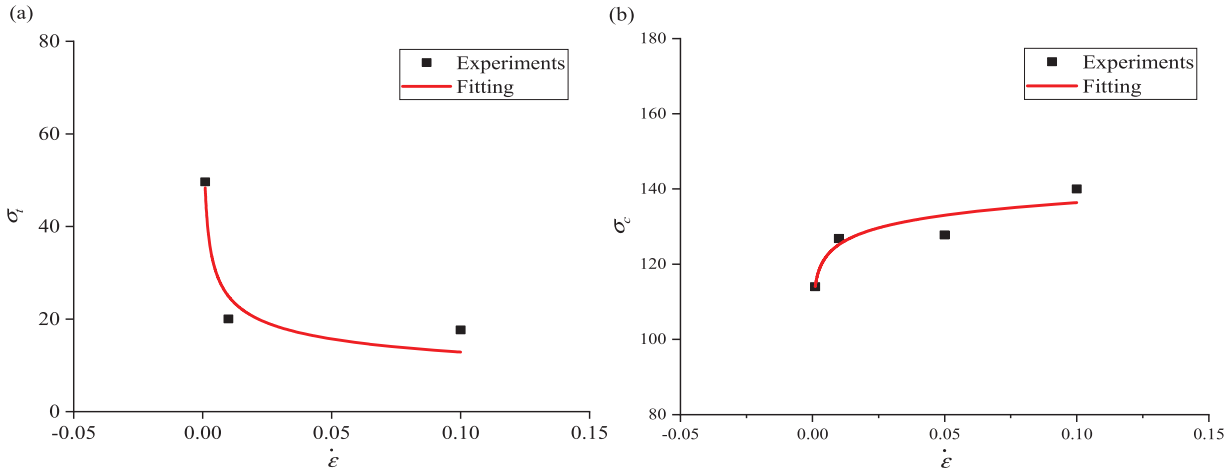

Figure 6. Relationship between yield stress and strain rate under (a) tensile and (b) compressive loading

Table 2. Yield stress parameters in tension and compression

Experiment type	**Tensile loading**			**Compressed loading**		
Parameters	a_t	b_t	R_t^2	a_c	b_c	R_c^2
Value	6.632	−0.287	0.923	147.529	11.160	0.999

4.2. Constitutive model of EP under tension

Through analysis, we found that the relationship between modulus and strain rate is an exponential function type curve, which is described here using the Asymptotic1 function. The fitting results are shown in Figure 7. The relationship between modulus and strain rate is

$$E_t = a - b \cdot c^{\dot{\varepsilon}} \tag{8}$$

The parameter values in Eq. (8) are: $a = 848.609$, $b = 0.045$, $c = 0.073$. Based on Hooke's law, the relationship between modulus and stress-strain can be used to establish a mechanical constitutive model for EP under tension.

The obtained constitutive model can predict the tensile stress-strain curves of EP at strain rates of 0.001, 0.01, and 0.1 s^{-1}, and compare them with the experimental stress-strain curves to verify the effectiveness. The initial nonlinear segment caused by the clamping end of the instrument is ignored here. It can be found that the predicted results are in good agreement with the experimental results in the linear segment, as shown in Figure 8a. Based on this constitutive model, the stress-strain behavior of EP under tensile load at strain rates of 0.005, 0.05, 0.5, 1 s^{-1}, and 5 s^{-1} is predicted, and the predicted

results are shown in Figure 8b. It can be seen from the figure that when the strain rate exceeds a certain range, the influence of the modulus becomes insignificant, but the strength gradually decreases. The constitutive equation is expressed as Eq. (9), namely

$$\sigma_t = E_t\varepsilon = \left[848.609 - 0.045 \cdot (0.073)^{\dot{\varepsilon}}\right] \cdot \varepsilon \tag{9}$$

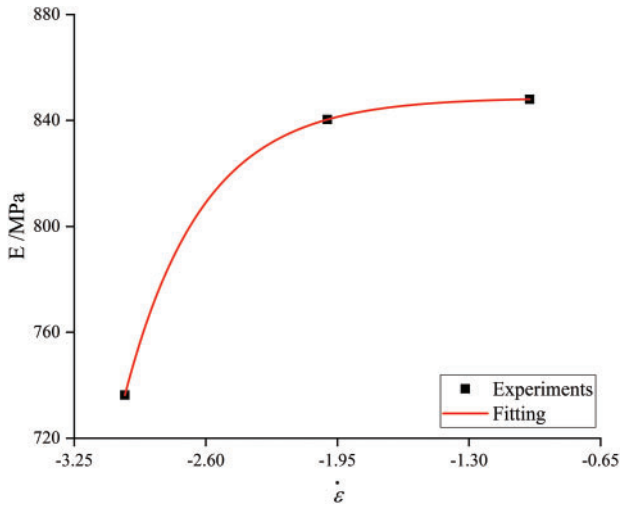

Figure 7. Relationship between modulus and strain rate under tension

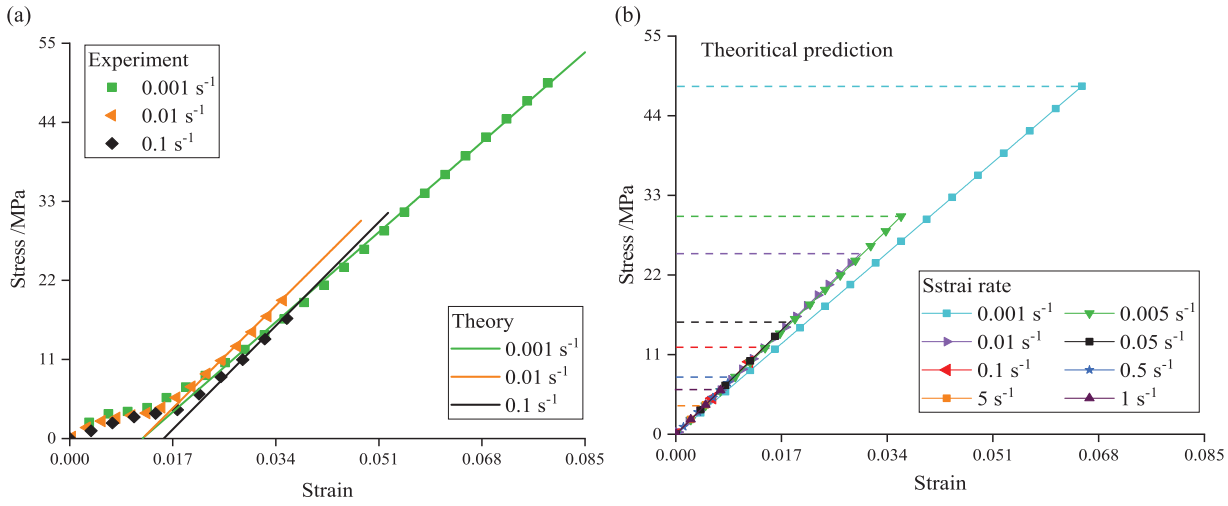

Figure 8. Validation and application of the models. (a) predicted tensile behavior compared to experimental results, where the initial phase is discarded, and (b) predicted tensile behavior for other strain rate conditions

4.3. Compressive constitutive model based on the sherwood-frost model

There are many studies on the compressive constitutive model of EP [14,15,17,18]. Among them, the mechanical behavior described by the constitutive model proposed by Sherwood et al. has a good correlation with our compression test results. Therefore, it was selected for constitutive modelling in the compressed state. The Sherwood-Frost constitutive model expresses the true stress of the material as a

combination of the shape function $f(\varepsilon)$, temperature function $H(T)$, density function $G(\rho)$ and strain rate function $M(\varepsilon, \dot{\varepsilon})$ [34], that is

$$\sigma_c = H(T)G(\rho)M(\varepsilon, \dot{\varepsilon})f(\varepsilon) \tag{10}$$

where $f(\varepsilon)$ is a polynomial function describing the shape of the stress-strain curve under the reference state, which is given by

$$f(\varepsilon) = \sum_{n=1}^{k} A_n \varepsilon^n \tag{11}$$

Under the condition of reference strain rate $\dot{\varepsilon}_{c0}$, strain rate function $M(\varepsilon, \dot{\varepsilon}_{c0}) = 1$, discarding temperature and density terms, then

$$\sigma_{c0} = f(\varepsilon) = \sum_{n=1}^{10} A_n \varepsilon^n \tag{12}$$

where $\dot{\varepsilon}_{c0}$ represents the minimum strain rate of the compression test. On this basis, the true stress-strain curve of EP when the strain rate is $\dot{\varepsilon}_c = \dot{\varepsilon}_{c0} = 0.001\ s^{-1}$ was fitted using the polynomial function, and the fitting results are shown in Figure 9, and the parameters of $f(\varepsilon)$ are given in Table 3. Therefore, the polynomial function $f(\varepsilon)$ can be obtained, namely

$$\sigma_{c0} = f(\varepsilon) = -12.056 + 3535.876\varepsilon - 34606.125\varepsilon^2 + 139116.814\varepsilon^3 - 187654.343\varepsilon^4 \tag{13}$$

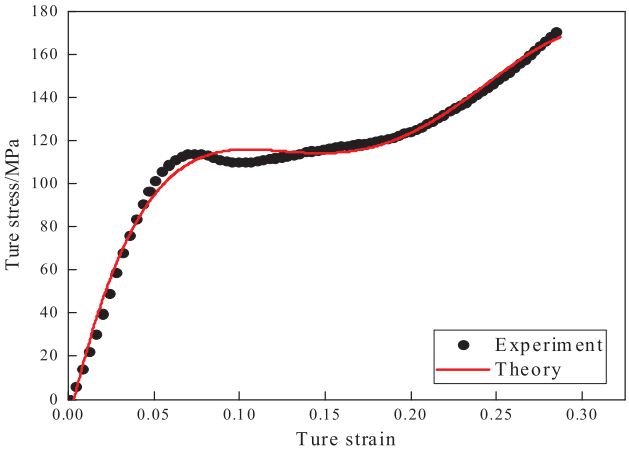

Figure 9. Compressive stress-strain curves including fit result using $f(\varepsilon)$ function and experimental result with strain rate 0.001 s^{-1}

Table 3. Material parameters of A_n in $f(\varepsilon)$ polynomial function

Compression ($k = 4$)	Parameters	A_{c0}	A_{c1}	A_{c2}	A_{c3}	A_{c4}
	Value	−12.056	3535.876	−34,606.125	139,116.814	−187,654.343

In Eq. (10), $M(\varepsilon, \dot{\varepsilon})$ is the exponential strain rate term proposed by Nagy et al. [35], which is expressed as

$$M(\varepsilon, \dot{\varepsilon}) = (\dot{\varepsilon}/\dot{\varepsilon}_0)^{n(\varepsilon)} \tag{14}$$

$$n(\varepsilon) = b_1 + b_2\varepsilon + b_3\varepsilon^2 + b_4\varepsilon^3 + b_5\varepsilon^4 \tag{15}$$

where, the material parameter $b_1 \sim b_5$ are determined by experiment, and have a unit of 1. Here the specific form of Eq. (10) is

$$\sigma_c = M(\varepsilon, \dot{\varepsilon}) f(\varepsilon) \tag{16}$$

In order to obtain the relationship between $M(\varepsilon, \dot{\varepsilon})$ and strain ε, we rewrite Eq. (16) as follows [36]:

$$M(\varepsilon, \dot{\varepsilon}) = \frac{\sigma_c}{f(\varepsilon)} = \frac{\sigma_c}{\sigma_{c0}} \tag{17}$$

Taking the strain rate of 0.001 s^{-1} as the reference strain rate, the relationship between $M(\varepsilon, \dot{\varepsilon})$ and strain ε can be obtained by Eq. (17), and the fitting results are shown in Figure 10.

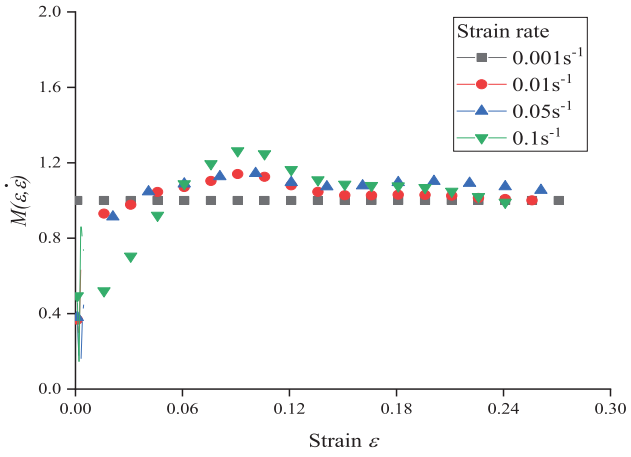

Figure 10. Relationship between $M(\varepsilon, \dot{\varepsilon})$ and ε under different strain rates the compression state

To obtain the parameter of $n(\varepsilon)$ in Eq. (14), take the logarithm of both sides of Eq. (14), then we can obtain

$$n(\varepsilon) = \frac{\ln[M(\varepsilon, \dot{\varepsilon})]}{\ln(\dot{\varepsilon}/\dot{\varepsilon}_0)} \tag{18}$$

Combining Figure 10 and Eq. (18) for calculation, the relationship between $n(\varepsilon)$ and strain is obtained, as shown in Figure 11. It can be seen that there is a nonlinear relationship between $n(\varepsilon)$ and strain ε. At the same time, the fitted curve is in good agreement with the experimental results. The parameter values in $n(\varepsilon)$ are given in Table 4, and its equation the compressive state is

$$n(\varepsilon)_c = -0.185 + 6.989\varepsilon - 73.814\varepsilon^2 + 312.358\varepsilon^3 - 466.129\varepsilon^4 \tag{19}$$

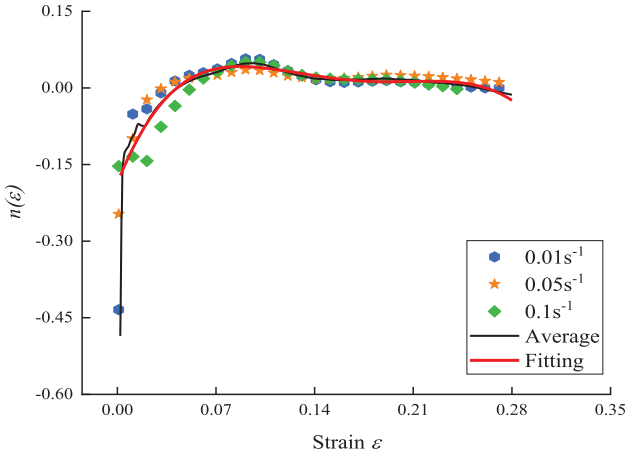

Figure 11. Relationship between $n(\varepsilon)$ and strain ε in compression state

Table 4. Experimental constants in $n(\varepsilon)$

Compression	Parameter	b_1	b_2	b_3	b_4	b_5
	Value	−0.185	6.989	−73.814	312.358	−466.129

According to the obtained shape function $f(\varepsilon)$ and strain rate function $M(\varepsilon, \dot{\varepsilon})$, combined with $n(\varepsilon)$, we can obtain the stress-strain constitutive model of EP under compression, that is

$$\begin{cases} \sigma_c = \left(\dot{\varepsilon}/\dot{\varepsilon}_{c0}\right)^{n(\varepsilon)_c} \cdot f(\varepsilon) \\ n(\varepsilon)_c = -0.185 + 6.989\varepsilon - 73.814\varepsilon^2 + 312.358\varepsilon^3 - 466.129\varepsilon^4 \\ f(\varepsilon) = -12.056 + 3535.876\varepsilon - 34606.125\varepsilon^2 + 139116.814\varepsilon^3 - 187654.343\varepsilon^4 \end{cases} \tag{20}$$

Compared with the experimental results, the compressive mechanical behaviors at different strain rates can be predicted based on the obtained constitutive model. Figure 12a to d shows the comparison between the stress-strain curve calculated based on the constitutive model Eq. (20) under compression and the experimental results. It can be found that the predicted results are in good agreement with the experimental results. Furthermore, we calculated the stress-strain curves of EP at strain rates of 0.005, 0.5, 10 and 100 s^{-1}, as shown in Figure 12e. It can be seen that as the strain rate increases, the failure strength increases, the modulus increases, the flow stress increases, but the overall trends of these are the same. However, the platform stability decreases. In summary, this constitutive model can be used to predict the compressive mechanics of EP at different strain rates.

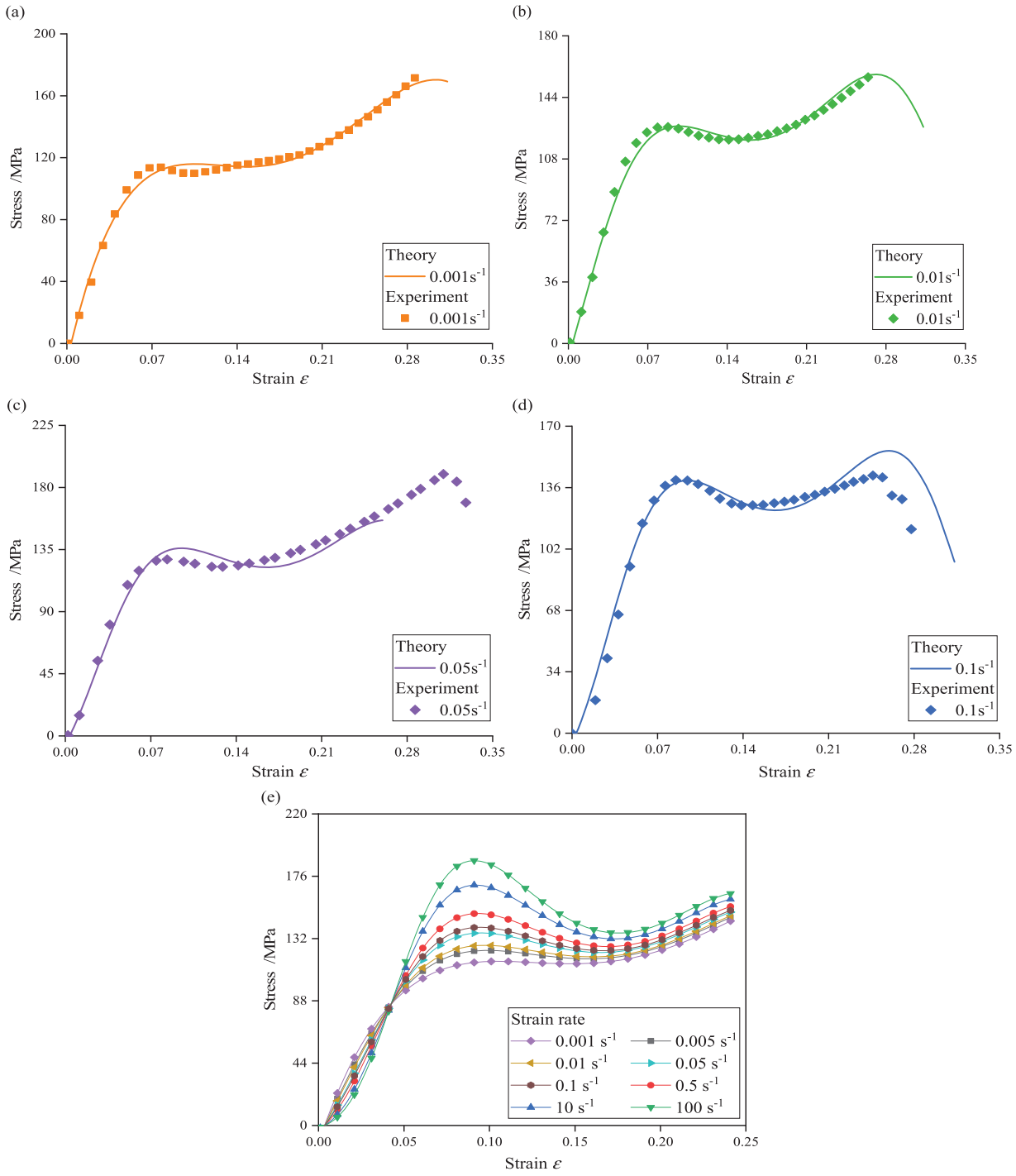

Figure 12. Validation and application of the models. Stress-strain prediction results compared to experimental results at strain rates of (a) 0.001 s^{-1}, (b) 0.01 s^{-1}, (c) 0.05 s^{-1}, (d) 0.1 s^{-1}, and (e) prediction results at other strain rates

4.4. Tensile constitutive model based on the sherwood-frost model

By observing the stress-strain curve of the material under tension, due to the existence of the initial nonlinear segment, a quadratic polynomial is used to fit the stress-strain curve. It is assumed here that there is an initial nonlinearity in the tensile behavior, otherwise, the polynomial function $f(\varepsilon)$ is useless. The result is shown in Figure 13, and the parameters of the shape function $f(\varepsilon)$ are given the Table 5,

and the polynomial function $f(\varepsilon)$ is

$$\sigma_{t0} = f(\varepsilon) = 0.748 + 234.879\varepsilon + 7834.590\varepsilon^2 \tag{21}$$

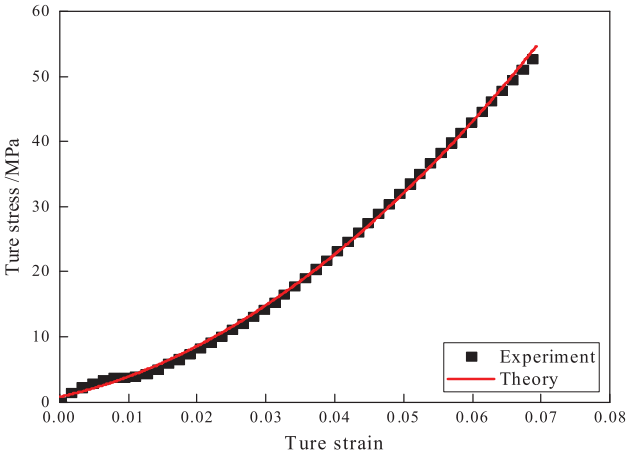

Figure 13. Tensile stress-strain curve experimental result and its $f(\varepsilon)$ fitting result

Table 5. Material parameters of An in the polynomial function $f(\varepsilon)$

Tensile condition ($k = 2$)	Parameter	A_{t0}	A_{t1}	A_{t2}
	Value	0.748	234.879	7834.590

Taking the strain rate of 0.001 s^{-1} as the reference strain rate, the relationship between $M(\varepsilon, \dot{\varepsilon})$ and strain ε under tension can be obtained through Eq. (17), and the calculation results are shown in Figure 14.

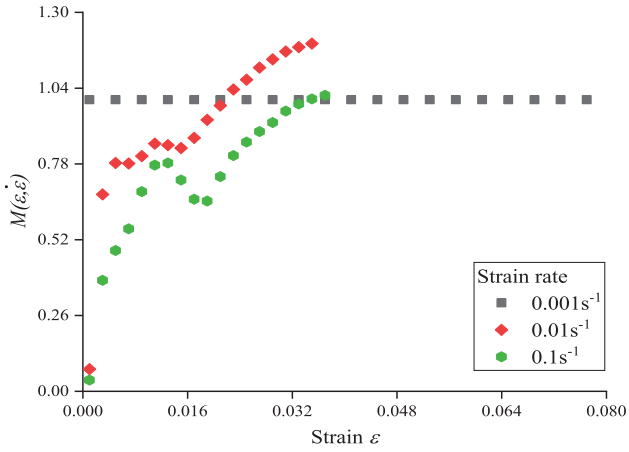

Figure 14. Relationship between $M(\varepsilon, \dot{\varepsilon})$ and ε under different strain rates in the tensile state

Combining Figure 14 and Eq. (18) for calculation, the relationship between $n(\varepsilon)$ and strain ε is obtained, where the fitting result is shown in Figure 15 and the parameters in $n(\varepsilon)$ are shown in Table 6.

The equation of $n\,(\varepsilon)$ in tensile state is

$$n\,(\varepsilon)_t = -0.342 + 59.766\varepsilon - 4836.902\varepsilon^2 + 170222.058\varepsilon^3 - 2.053\varepsilon^4 \tag{22}$$

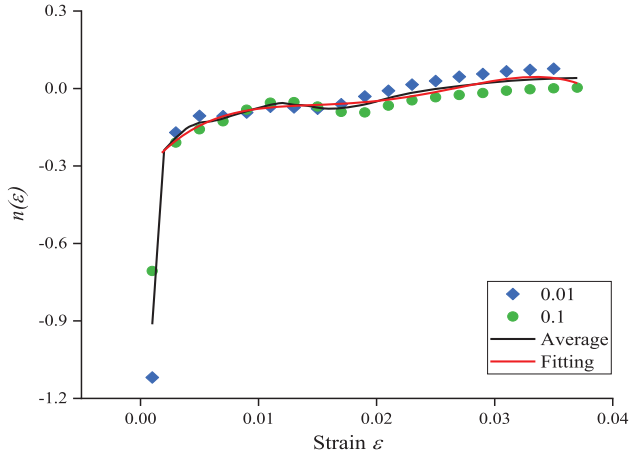

Figure 15. Relationship between $n\,(\varepsilon)$ and material strain ε under tension

Table 6. Experimental constants in $n\,(\varepsilon)$ in tension

Tensile condition	Parameters	b_1	b_2	b_3	b_4	b_5
	Value	−0.342	59.766	−4836.902	170,222.058	−2.053

Similarly, the constitutive model of EP in the Sherwood-Frost form under tension can be obtained, namely

$$\begin{cases} \sigma_t = \left(\dot{\varepsilon}/\dot{\varepsilon}_{t0}\right)^{n(\varepsilon)_t} \cdot f\,(\varepsilon) \\ n\,(\varepsilon)_t = 0.748 + 234.879\varepsilon + 7834.590\varepsilon^2 \\ f\,(\varepsilon) = -0.342 + 59.766\varepsilon - 4836.902\varepsilon^2 + 170222.058\varepsilon^3 - 2.053\varepsilon^4 \end{cases} \tag{23}$$

Then, we can discuss its predictive effect. After the calculation, the theoretical prediction results were compared with the experimental results and other predictions under tension, as shown in Figure 16. The results show that the predictions in the initial segment are consistent with the experimental results. However, the predictions in the subsequent linear segment are inaccurate. This is because there are two nonlinear terms in the constitutive equation, namely $f\,(\varepsilon)$ and $n\,(\varepsilon)$. In addition, according to the relationship in Figure 14, it can be seen that the regularity of the three $M\,(\varepsilon, \dot{\varepsilon})$ is poor, and their fitting results are nonlinear. As a result, although a nonlinear assumption is introduced for the constitutive establishment, the obtained nonlinear Sherwood-Frost model cannot reflect the linear elastic behavior well. Therefore, for the prediction of mechanical behavior under tension, the simple constitutive model of Eq. (9) in Section 4.2 is more appropriate, as it has a better predictive effect on the overall mechanical behavior.

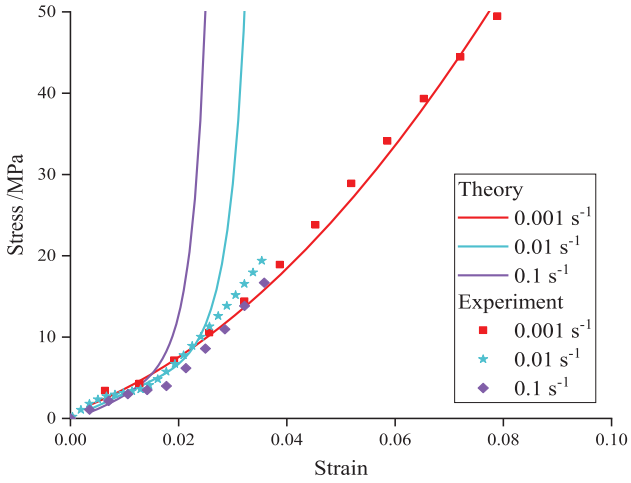

Figure 16. Predicted and experimental results of stress-strain curves under tension

As a result, the complete constitutive model of EP under tension and compression is

$$\begin{cases} \text{tension}: \ \sigma_t = \left[848.609 - 0.045 \cdot (0.073)^{\dot{\varepsilon}}\right] \cdot \varepsilon \\ \text{compression} \begin{cases} \sigma_c = \left(\dot{\varepsilon}/\dot{\varepsilon}_{c0}\right)^{n(\varepsilon)_c} \cdot f(\varepsilon) \\ n(\varepsilon)_c = -0.185 + 6.989\varepsilon - 73.814\varepsilon^2 + 312.358\varepsilon^3 - 466.129\varepsilon^4 \\ f(\varepsilon) = -12.056 + 3535.876\varepsilon - 34606.125\varepsilon^2 + 139116.814\varepsilon^3 - 187654.343\varepsilon^4 \end{cases} \end{cases} \tag{24}$$

5. Conclusion

EP has an obvious strain rate effect and strength-difference effect under tension-compression loading. This indicates that the form of applied load should be considered when studying its mechanical behavior. In this paper, we have studied the uniaxial tensile and compressive behavior of EP under different low strain rates by quasi-static tests, and established the constitutive models. The main conclusions are:

(1) For the tensile test of EP, the results show that there is a negative correlation between yield stress and strain rate, and the elastic modulus increases with increasing strain rate. The prediction results obtained from the established simple constitutive model are in good agreement with the experimental results.

(2) For the compression test of EP, the results show that both yield stress and elastic modulus increase with increasing strain rate. The results of predicting the mechanical behavior based on the Sherwood-Frost constitutive model are in good agreement with the experimental results, among which the nonlinear terms of the shape function, strain rate function, and strain rate exponential function together constitute the nonlinear elastoplastic behavior under compression.

(3) The results at different strain rates show that the mechanical behavior of EP is strain rate dependent. For the mechanical properties of EP in tension and compression at the same strain rate, the yield strength, elastic modulus, and plastic behavior show obvious differences, that is, a strength-difference effect under tension and compression, and the compressive behavior has an obvious plastic flow phase.

(4) The Sherwood-Frost constitutive model is not suitable for the mechanical properties of EP under tension, which is mainly manifested by the fact that the constitutive model has two polynomial nonlinear terms, namely $f(\varepsilon)$ and $n(\varepsilon)$. This indicates that the nonlinear Sherwood-Frost model has a drawback in

predicting the linear behavior, thus the simple linear model is more appropriate for the tensile mechanics of EP.

Although this paper has discussed the tensile and compressive behavior of EP at a strain rate of 0.001 to 0.1 s^{-1} and established tensile and compressive constitutive models, the prediction of tensile and compressive behavior at other strain rate conditions is not supported by experimental data. In the future, the mechanical behavior of EP at strain rates of 0.005, 0.5, 5, 10, 50 and 100 s^{-1} can be further discussed. In addition, the constitutive model established in this paper is still a theoretical equation and needs further development to form a material subroutine that can be used in numerical simulations.

Acknowledgement: The authors gratefully acknowledged the financial support from the Key Research and Development Program of Heilongjiang Province (Grant number: 2023ZX07D03, corresponding to Hao Liu).

Author Contributions: Changlin Zhao: Writing—original draft preparation, Investigation, Methodology, Conceptualization, Data curation, Software, Formal analysis. Hao Liu: Writing—reviewing and editing, Investigation, Conceptualization, Funding. All authors reviewed the results and approved the final version of the manuscript.

Availability of Data and Materials: The raw/processed data required to reproduce these findings cannot be shared at this time as the data also forms part of another study.

Conflicts of Interest: The authors declare no conflicts of interest to report regarding the present study.

References

1. JIN, F., LI, X., PARK, S., Synthesis and application of epoxy resins: a review. *J. Indust. Eng. Chem.*, 29, 2015, 1–11. https://doi.org/10.1016/j.jiec.2015.03.026.
2. JAMS IFAN, B., WINDSOR FREDRIC, M., THOMAS POUDEVIGNE, D., ORMEROD STEVE, J., ANDDURANCE, I., Estimating the size distribution of plastics ingested by animals. *Nat. Communicat.*, 11(1), 2020, 1594. https://doi.org/10.1038/s41467-020-15406-6.
3. NIU, P., ZHAO, Z., ZHU, J., ZHANG, Z., SUN, A. et al., Epoxy-based multifunctional re-bondable polymer with self-healing, shape memory and superb bonding properties. *J. Coll. Interf. Sci.*, 678(7704), 2025, 30–39. https://doi.org/10.1016/j.jcis.2024.08.243.
4. NABAVIAN KALAT, M., ZIAI, Y., DZIEDZIC, K., GRADYS, A., URBAŃSKI, L. et al., Experimental evaluation of build orientation effects on the microstructure, thermal, mechanical, and shape memory properties of SLA 3D-printed epoxy resin. *Eur. Poly. J.*, 228, 2025, 113829. https://doi.org/10.1016/j.eurpolymj.2025.113829.
5. ZHAO, C., MENG, Z., YI, J., CHEN, C. Q., Auxetic metamaterials with double re-entrant configuration. *Int. J. Mech. Sci.*, 301(3), 2025, 110505. https://doi.org/10.1016/j.ijmecsci.2025.110505.
6. YAO, S. S., JIN, F. L., RHEE, K. Y., HUI, D., PARK, S. J., Recent advances in carbon-fiber-reinforced thermoplastic composites: a review. *Compos. Part B: Eng.*, 142, 2018, 241–250. https://doi.org/10.1016/j.compositesb.2017.12.007.
7. LITTELL, J. D., CHARLES, R. R., GOLDBERG, R. K., ROBERTS, G. D., WILLIAM, A. A. et al., Measurement of epoxy resin tension, compression, and shear stress-strain curves over a wide range of strain rates using small test specimens. *J. Aerosp. Eng.*, 21(3), 2008, 162–173. https://doi.org/10.1061/(asce)0893-1321(2008)21:3(162).
8. CHEN, W., LU, F., CHENG, M., Tension and compression tests of two polymers under quasi-static and dynamic loading. *Polym. Test.*, 21(2), 2002, 113–121. https://doi.org/10.1016/s0142-9418(01)00055-1.
9. LJ, C., ANDISHAI, O., Strain-rate dependence of the elastic modulus of filled and porous epoxy composites. *Int. J. Mech. Sci.*, 9(9), 1967, 605–608. https://doi.org/10.1016/0020-7403(67)90065-3.

10. GÓMEZ DEL RÍO, T., RODRÍGUEZ, J., PEARSON, R. A., Compressive properties of nanoparticle modified epoxy resin at different strain rates. *Compos. Part B: Eng.*, 57, 2014, 173–179. https://doi.org/10.1016/j.compositesb.2013.10.002.
11. ISHAI, O., Delayed yielding of epoxy resin under tension, compression, and flexure. I. Behavior under constant strain rate. *J. Appl. Polym. Sci.*, 11(6), 1967, 963–981. https://doi.org/10.1002/app.1967.070110616.
12. TAMRAKAR, S., GANESH, R., SUBRAMANI, S., HAQUE, B. Z., ANDJOHN, W. G., Experimental investigation of strain rate and temperature dependent response of an epoxy resin undergoing large deformation. *J. Dynam. Behav. Mat.*, 4(1), 2018, 114–128. https://doi.org/10.1007/s40870-018-0144-8.
13. ZHONG, J., REN, R., TANG, Z., REN, J., ZHAO, C., Analysis of nonlinear mechanical behavior of resin materials at low and medium strain rates. *Polym. Compos.*, 43(6), 2022, 3699–3707. https://doi.org/10.1002/pc.26647.
14. ZHU, Z., XU, D., WANG, L., Thermoviscoelastic constitutive equation and time-temperature equivalence of epoxy resins at high strain rates. *J. Ningbo Univ. (Sci. Eng.)*, 1(1), 1988, 58–68. (In Chinese).
15. NING, R., Tensile stress-strain behavior of epoxy castings. *Eng. Plast. Applicat.*, (1), 1987, 38–41. (In Chinese).
16. WU, C. Dynamic mechanical behavior and constitutive model of epoxy resin at different temperatures [master's thesis]. Nanjing, China: Nanjing University of Aeronautics and Astronautics; 2020. (In Chinese).
17. COLAK, O. U., CAKIR, Y., Material model parameter estimation with genetic algorithm optimization method and modeling of strain and temperature dependent behavior of epoxy resin with cooperative-VBO model. *Mech. Mat.*, 135(2), 2019, 57–66. https://doi.org/10.1016/j.mechmat.2019.04.023.
18. THEOCARIS, P. S., Viscoelastic properties of epoxy resins derived from creep and relaxation tests at different temperatures. *Rheolo. Acta*, 2(2), 1962, 92–96. https://doi.org/10.1007/bf01972534.
19. ZHAO, C. H., ZHANG, G. C., SUN, W. M., ANDAI, H. S., Study on processing properties of epoxy resin system in VARI. *Adv. Mat. Res.*, 463–464, 2012, 704–707. https://doi.org/10.4028/www.scientific.net/AMR.463-464.704.
20. SUN, W., GUAN, Z., LI, Z., ZHANG, M., HUANG, Y., Compressive failure analysis of unidirectional carbon/epoxy composite based on micro-mechanical models. *Chin. J. Aeronaut.*, 30(6), 2017, 1907–1918. https://doi.org/10.1016/j.cja.2017.10.002.
21. ZHAO, C., HE, Y., Experimental study on tensile and epoxy resin compressive mechanics of plain carbon fiber composites. *J. Ordn. Equip. Eng.*, 43(6), 2022, 309–316. (In Chinese).
22. KOERBER, H., XAVIER, J., CAMANHO, P. P., High strain rate characterisation of unidirectional carbon-epoxy IM7-8552 in transverse compression and in-plane shear using digital image correlation. *Mech. Mat.*, 42(11), 2010, 1004–1019. https://doi.org/10.1016/j.mechmat.2010.09.003.
23. XIA, L., LV, Q., LI, Z., Study on the constitutive relationship of resin castings at different temperatures. *FRP/Composites*, (3), 2011, 24–27. (In Chinese).
24. LIU, Z., ZHONG, J., REN, R., TANG, Z., ZHAO, C. et al., Nonlinear mechanical behavior of glass fiber/epoxy resin composite under medium and low strain rates loading. *Appl. Compos. Mat.*, 31(4), 2024, 1369–1392. https://doi.org/10.1007/s10443-024-10233-0.
25. AMOS, G., ROBERT, K. G., GARY, D. R., Experimental study of strain-rate-dependent behavior of carbon/epoxy composite. *Compos. Sci. Technol.*, 62(10–11), 2002, 1469–1476. https://doi.org/10.1016/S0266-3538(02)00100-8.

26. SHOKRIEH, M. M., OMIDI, M. J., Tension behavior of unidirectional glass/epoxy composites under different strain rates. *Compos. Struct.*, 88(4), 2009, 595–601. https://doi.org/10.1016/j.compstruct.2008.06.012.
27. ZHANG, M., YU, Y., LI, L., ZHOU, H., GONG, L., ZHOU, H., A molecular dynamics assisted insight on damping enhancement in carbon fiber reinforced polymer composites with oriented multilayer graphene oxide coatings. *Microstructures*, 4(4), 2024, 2024051. https://doi.org/10.20517/microstructures.2024.29.
28. ZHONG, J., ZHAO, C., CHEN, C., LAI, W. L., WANG, Q., Mechanical behaviors of composite auxetic structures under quasi-static compression and dynamic impact. *Eu. J. Mech.-A/Sol.*, 109(5), 2025, 105454. https://doi.org/10.1016/j.euromechsol.2024.105454.
29. ZHAO, C., ZHONG, J., WANG, H., LIU, C., LI, M. et al., Impact behaviour and protection performance of a CFRP NPR skeleton filled with aluminum foam. *Mat. Des.*, 246, 2024, 113295. https://doi.org/10.1016/j.matdes.2024.113295.
30. KAMAYA, M., KAWAKUBO, M., A procedure for determining the true stress-strain curve over a large range of strains using digital image correlation and finite element analysis. *Mech. Mat.*, 43(5), 2011, 243–253. https://doi.org/10.1016/j.mechmat.2011.02.007.
31. YAMINI, S., YOUNG, R. J., Stability of crack propagation in epoxy resins. *Polymer*, 18(10), 1977, 1075–1080. https://doi.org/10.1016/0032-3861(77)90016-7.
32. HU, H., HUANG, S., WANG, S., YE, L., LIU, K, Dynamic compressibility of two-component epoxy casting systems. In: The 8th Member Congress of Anhui Mechanical Engineering Society and the 50th Anniversary Celebration of the Society; 1 December 2014; 2014; Xi'an, China. p. 399–401. (In Chinese).
33. ZHANG, K., LI, W., YU, Z., YAO, W., ZHAO, C., Compressive properties and constitutive model of semicrystalline polyethylene. *Polymers*, 13(17), 2021, 2895. https://doi.org/10.3390/polym13172895.
34. JAMES, A. S., COLIN, C. F., Constitutive modeling and simulation of energy absorbing polyurethane foam under impact loading. *Polym. Eng. Sci.*, 32(16), 1992, 1138–1146. https://doi.org/10.1002/pen.760321611.
35. NAGY, A., KO, W. I., LINDHOLM, U. S., Mechanical behavior of foamed materials under dynamic compression. *J. Cellular Plast.*, 10(3), 1974, 127–134. https://doi.org/10.1177/0021955X74010003.
36. ZHANG, K., LI, W., ZHENG, Y., YAO, W., ZHAO, C., Dynamic constitutive model of ultra-high molecular weight polyethylene (UHMWPE): considering the temperature and strain rate effects. *Polymers*, 12(7), 2020, 1561. https://doi.org/10.3390/polym12071561.

Received: 04 March 2025; Accepted: 26 June 2025; Published: 18 July 2025